Impact of Phosphorylation on the Structural Ensemble of alpha-Synuclein in Aqueous Solution

Anton Emil Dorn,[†,‡,¶] Emile de Bruyn,[†,‡,§] Giulia Rossetti,[*,‡,∥,⊥] Claudio Fernandez,[#,@] Tiago F. Outeiro,[△,∇,††] Jörg B. Schulz,[§,⊥,‡‡] and Paolo Carloni[§,∥]

† *Equally contributed to this work*
‡ *Jülich Supercomputing Centre (JSC), Forschungszentrum Jülich GmbH, 52425 Jülich, Germany*
¶ *Faculty of Biology, University of Duisburg-Essen, 45141 Essen, Germany*
§ *Department of Physics, RWTH Aachen University, 52062 Aachen, Germany*
∥ *Computational Biomedicine (IAS-5/INM-9), Forschungszentrum Jülich GmbH, 52425 Jülich, Germany*
⊥ *Department of Neurology, RWTH Aachen University, 52074 Aachen, Germany*
\# *Max Planck Laboratory for Structural Biology, Chemistry and Molecular Biophysics of Rosario (MPLbioR, UNR-MPINAT). Partner of the Max Planck Institute for Biophysical Chemistry (MPINAT, MPG). Centro de Estudios Interdisciplinarios, Universidad Nacional de Rosario, S2002LRK Rosario, Argentina*
@ *Department of NMR-based Structural Biology, Max Planck Institute for Multidisciplinary Sciences, 37077 Göttingen, Germany*
△ *Department of Experimental Neurodegeneration, Center for Biostructural Imaging of Neurodegeneration, University Medical Center Göttingen, 37075 Göttingen, Germany*
∇ *Max Planck Institute for Multidisciplinary Sciences, 37075 Göttingen, Germany*
†† *Translational and Clinical Research Institute, Newcastle University, Newcastle upon Tyne NE1 7RU, United Kingdom*
‡‡ *JARA Brain Institute Molecular Neuroscience and Neuroimaging (INM-11), Research Centre Jülich and RWTH Aachen University, 52074 Aachen, Germany*

E-mail: g.rossetti@fz-juelich.de

Abstract

Serine 129 can be phosphorylated in pathological inclusions formed by the intrinsically disordered protein α-synuclein (AS), a key player in Parkinson's disease and other synucleinopathies. Here, molecular simulations suggest that phosphorylation does not impact on the structural ensemble of the physiological AS conformational ensemble in

aqueous solution, as the phosphate group is mostly solvated. Our findings are consistent with experimental data, with the caveat that the latter are carried out on the non-acetylated, non-physiological form of the protein. These findings shed light into the molecular implications of AS phosphorylation and this may open novel perspectives for therapeutic intervention.

1 Introduction

Parkinson's disease (PD) is the second most common neurodegenerative disease after Alzheimer's disease,[1] affecting several million people worldwide.[2,3] The typical pathological hallmark is the accumulation of fibrillar protein inclusions, know as Lewy bodies (LBs) and Lewy neurites (LNs) in the brain.[4,5] The major component of LBs and LNs are fibrillar forms of the human α-synuclein (AS) protein.[3,6] AS is a 140 amino acid 'disordered' conformational ensemble both in aqueous solution and in vivo. AS acquires some degree of structure when bound to the membrane or to cellular partners.[7,8]

The primary sequence of AS can be divided in three domains: the positively charged N-terminus (residues 1-60), the overall neutral non-amyloid component (NAC) region (residues 61-95) and the negatively charged C-terminal domain (residues 96-140, Figure 1). Under physiological conditions, the protein is acetylated on the first residue, although in vitro studies suggest this N-terminal acetylation does not significantly change the fibrillization propensity in vitro.[9] In LBs, a significant fraction of AS is phosphorylated on S129.[1] It is still unclear whether this post-translational modification (PTM) plays a pathological and/or physiological role.[10–13] However, recent data actually suggests S129 phosphorylation may be regulated by neuronal activity, suggesting that the process may be part of the normal physiology of AS.[14]

The formation of the S129-O-PO_3^{2-} group at the C-terminus instead of one of the other two domains is intriguing, because it introduces as many as two negative charges at physio-

[1] A novel phosphorylation site of α-synuclein at T64 has also been recently described.[9]

logical pH (the pKa_1 and pKa_2 of phosphoserine are < 2 and 5.6[15]).[2]

The impact of phosphorylation on the structural ensemble and aggregation propensity of AS is not known. The Circular Dichroisim (CD) spectra of the *non-N-term acetylated*, non physiological form of the protein[16,17] in solution points to significant changes in the structural ensemble. However, the structure of the physiological form differs from that of the non-acetylated one (which does not exist in human cells), so firm conclusions cannot be made from these studies.

```
MDVFMKGLSKAKEGVVAAAEKTKQGVAEAAGKTKE  35
GVLYVGSKTKEGVVHGVATVAEKTKEQVTNVGGAV  70
VTGVTAVAQKTVEGAGSIAAATGFVKKDQLGKNEE 105
GAPQEGILEDMPVDPDNEAYEMPSEEGYQDYEPEA 140
```

Figure 1: Sequence of amino acid residues in AS; positively charged residues are highlighted in blue and negatively charged ones in red. Three domains can be identified: the positively charged N-terminus (residues 1-60), the overall neutral non-amyloid component (NAC) region (residues 61-95) and the negatively charged C-terminal domain (residues 96-104). In physiological conditions, the protein is acetylated on the first residue, although this post-translational modification does not significantly affect the fibrillization propensity in vitro.[18] In LBs, a significant fraction of AS is phosphorylated on S129.[19] A novel phosphorylation site at T64 has also been recently described.[9]

Here, we investigate the impact of phosphorylation on the conformational ensemble of the physiological form of AS by molecular simulation. Our work builds upon our AMBER-based Replica Exchange with Solute Tempering 2 (REST2)[20] enhanced sampling predictions of wild-type[21,22] and mutants[22] of AS,[23] which turn out to reproduce a variety of biophysical properties of the protein.

To the best of the authors' knowledge, our molecular simulation studies are the only ones so far on the physiological form of AS in explicit solvent. Many molecular simulation studies, besides those in references,[24,25] focus on the non-acetylated protein.[26–28,28–49] The calculations are based on the DES-Amber ff99SB[50] and the AMBER a99SB-*disp* force fields,[24] which have been tailored for IDPs. Amber a99SB-*disp* has already been successfully used for the non-

[2]It might be possible that the phosphate is partially monoprotonated. The effect of protonation is discussed in the Supplementary Information.

acetylated form of the protein in the free form[24,48] and in the presence of ligands.[25] The conformational space of the protein was efficiently explored using our REST2 simulations and it was shown to reproduce a variety of biophysical properties of the protein.

The simulations presented here face the challenging doubly charged phosphate group. While the parameters for phosphorylated serine, threonine, and tyrosine are present in the most widely used force fields, including AMBER,[51,52] CHARMM,[53,54] and GROMOS,[55] some of these parametrizations have at times shown artifacts,[56,57] even quite recently.[58] Here, our calculations are based on (i) the DES-Amber force field, for which phosphate parameters have been calibrated based on osmotic coefficient calculations.[59] and (ii) the standard a99SB-*disp* Amber force-field[51,52] for the protein and the solvent, along with a specific, AMBER-compatible parametrization of the phosphate group[60]

2 Methods

2.1 Molecular Simulations

The initial structure of the acetylated protein (AS) which best reproduced the chemical shifts in ref. 61 was selected from the conformational ensemble previously reported in ref. 21. The phosphorylated protein (pAS) was built by adding a phosphate group to S129 using PyMOL.[62]

AS and pAS were inserted in a water-filled dodecahedral simulation box with periodic boundary conditions and minimum distance of 35 Å between the protein and the box edges. Na^+ and Cl^- ions were added to neutralize the system and achieve a concentration of $150\,\mathrm{mmol\,L^{-1}}$. Table 1 shows the composition of the systems.

Table 1: Number of atoms in the simulation box for the three systems simulated here.

	Protein	Water	Sodium	Chlorine
AS	2,020	190,533	186	176
pAS	2,023	172,359	171	159

The simulations were based on: (i) the DES-Amber force field[50] and the standard TIP4P-D water model[63] (Table S1 for a full list of the parameters used); (ii) the a99SB-*disp* force field[24] and its accompanying modified TIP4P-D water model.[24] Long range electrostatics were evaluated using the Particle-Mesh Ewald (PME) method,[64] using a cutoff distance of 12 Å in real space. The van der Waals interactions featured the same cutoff.

Constant temperature conditions were achieved by coupling the systems with a Nosé-Hoover thermostat[65] at 300 K, with a time constant of 0.5 ps. Constant pressure was achieved with a Parrinello-Rahman barostat[66] at 1 bar, with a time constant of 2 ps (Table S1). The LINCS algorithm was used for all bonds involving hydrogen atoms.[67] The equations of motions were integrated using the `md` leap-frog algorithm, with a timestep of 2 fs.

The proteins underwent energy minimization (Table S2), and, subsequently 100 ps of MD in the NVT ensemble (Table S3). Then, they were heated up in 25 ps-long steps of 5 K in the same ensemble up to 300 K using simulated annealing (Tables S4 and S5). The systems were further equilibrated for 1 ns in the NPT ensemble (Table S6). Finally, they underwent 100 ns REST2 simulations[20] in the NPT ensemble. The proteins were not found to be near their periodic images at distances lower than 12 Å during any of these simulations. The simulations converged after 12 ns (see Section 3).

Structurally similar conformational clusters were obtained following the method for clustering IDPs described in ref. 68: For both AS and pAS, a total of 8.000 frames from the converged trajectories were clustered (Figures S1 and S2).

The following properties were calculated for conformations after convergence: (i) The radius of gyration R_g, calculated using the MDTraj Python code.[69] (ii) The hydrodynamic radius, calculated from the radii of gyration using the linear fit of ref. 36. (iii) The NMR chemical shifts of the C_α atoms, calculated using the shiftx2 code.[70] (iv) The CD spectra, using the DichroCalc code.[71] Additionally the average of all conformational clusters, weighted to their occurrence along the trajectory, was calculated. (v) The solvent accessible surface area (SASA) using the MDTraj code.[69] (vi) The contact map of protein residues using mini-

mum pairwise distances between residues using the MDTraj code.[69] (vii) Radial distribution functions (RDFs) from the oxygen atoms of S129 using the SPEADI[72,73] code developed by the authors.

Hydrogen bonds were defined according to the scheme in ref. 74. These were identified using the MDTraj code.[69] (ix) Salt bridges were defined using a distance between two charged atoms in the protein at a distance below 3.25 Å as in ref. 75. The MDTraj code[69] was also used to identify these. Secondary structure elements were identified using MDTraj[69] and DSSP.[76]

3 Results and Discussion

We performed REST2 simulations[20] for 100 ns, using 32 replicas, for both AS and pAS in aqueous solution. The calculations were based on the DES-Amber and the a99SB-*disp* force fields. We report here the results for the first calculations, while the second can be found in the Supplementary Information.

Convergence. We calculated two quantities as a function of simulated time to investigate the convergence of the systems (Figures S3 to S6): (i) the running averages of the percentage of secondary structures. In particular, helix structures reached a plateau after 12 ns; (ii) the running averages of the C_α chemical shifts which converge closely to the experimental values within 12 ns. Because of the limitations of the standard usage of RMSD with IDPs such as AS,[77] the running RMSD of atomic positions was not taken into account. Based on this analysis, we calculated structural properties in the interval 12–100 ns.

Comparison with experiment. The computational setup results in trajectories that reproduce the experimental data (NMR, CD and hydrodynamic radius)[61,78,79] available for AS (Figures S5 to S7 and Table S8).

Effect of phosphorylation. The ten most frequent conformational clusters of AS and pAS represent a total of 47.7 % and 52.9 % of the converged simulation trajectories,

respectively (Table S7). They are presented in Figures 2 and 3.

The mean calculated hydrodynamic radii agree with the experimental values (28.2 and 35.3 Å for AS and pAS,[16] respectively), within the standard deviation (Table 2). These and the mean radii of gyration (R_g) decrease slightly upon phosphorylation (still within the margin of error, Table 2). The distribution of R_g, however, differs significantly between AS and pAS (Figure 4(a)): the latter displays a higher propensity for either compact or extended conformations than AS. At the qualitative level, this changes the free energy landscape of the protein to form two slightly deeper basins instead of a more shallow landscape (Figures 4(b) and 4(c)). Interestingly, pAS displays a higher likelihood to retain a compact conformation, even when the distance between the termini increases.

Table 2: Calculated properties of AS and pAS. (i) Hydrodynamic R_H and gyration (R_g) radii of the entire proteins and of the NAC regions. (ii) Average number of hydrogen bonds. (iii) Average number of salt bridges. Standard deviations are indicated in parenthesis.

Protein	R_H [Å]	R_g [Å]	R_g(NAC) [Å]	R_H(NAC) [Å]	n_{SB}	N_{HB}
AS	35.1 (± 6.1)	35.6 (± 12.8)	23.8 (± 16.4)	28.3 (± 11.3)	1.54 (± 1.23)	19.52 (± 4.28)
pAS	31.0 (± 5.8)	28.0 (± 9.6)	17.2 (± 9.2)	23.1 (± 8.1)	1.86 (± 1.75)	20.67 (± 4.32)

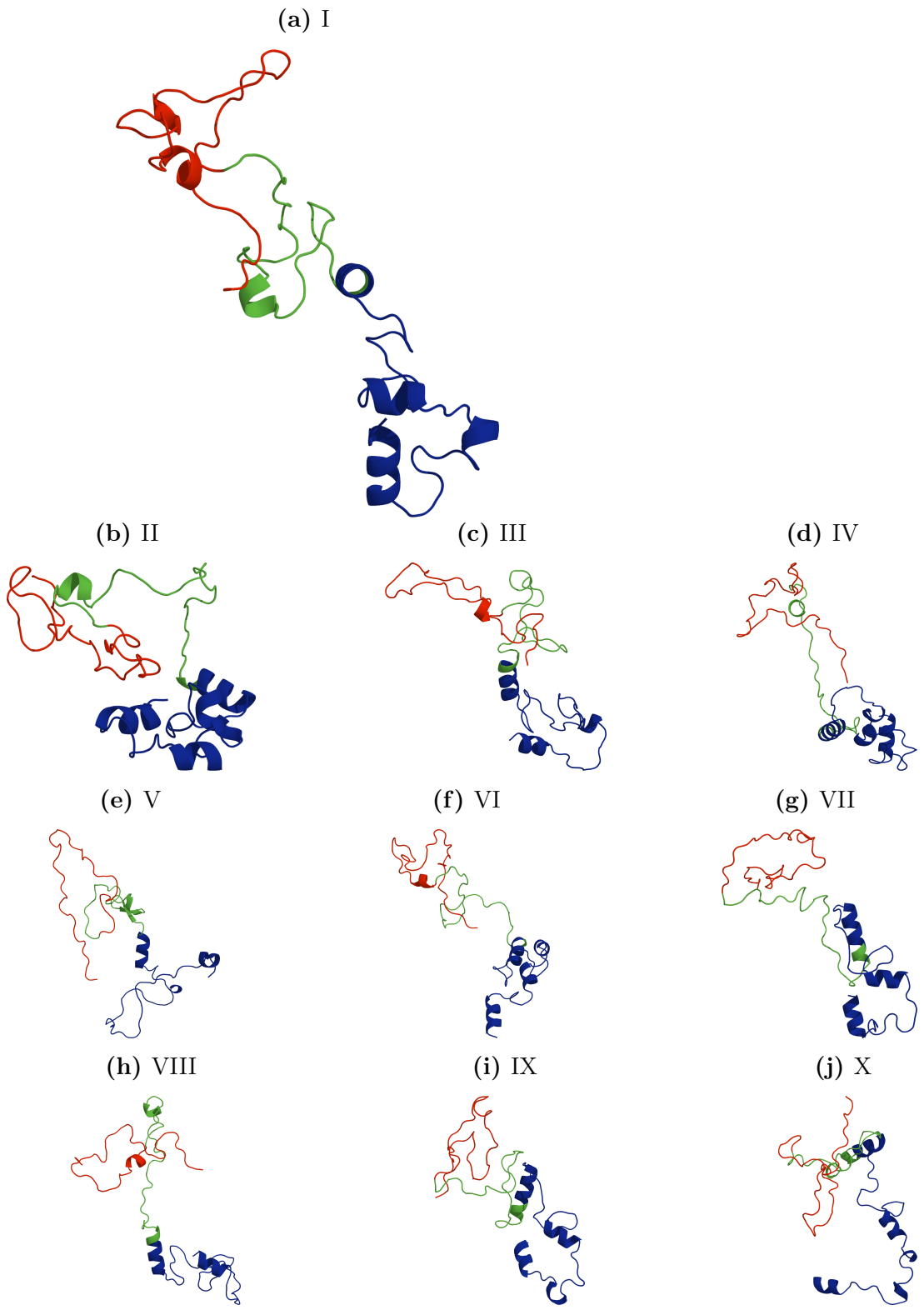

Figure 2: Representative structures (I-X) of AS as determined by clustering. The N-terminal domain is colored blue, the NAC domain green and the C-terminal domain red. The percentage of occurrence of the structures decreases from left to right and top to bottom (Table S7).

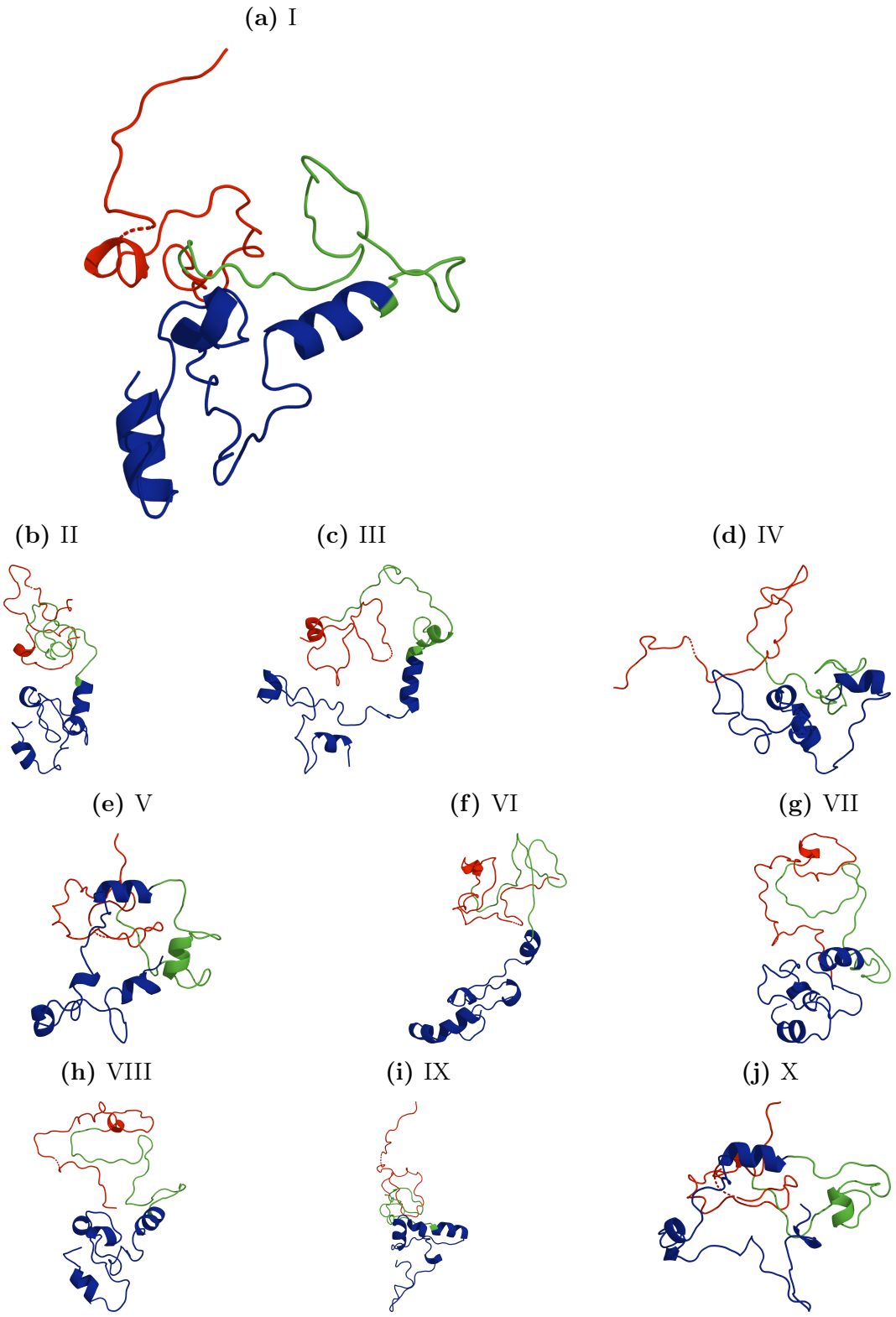

Figure 3: Representative structures (I-X) of pAS as determined by clustering. The acetyl group at the N-terminus and the residue at position S129 are shown as ball and sticks. The percentage of occurrence of the structures decreases from left to right and top to bottom (Table S7).

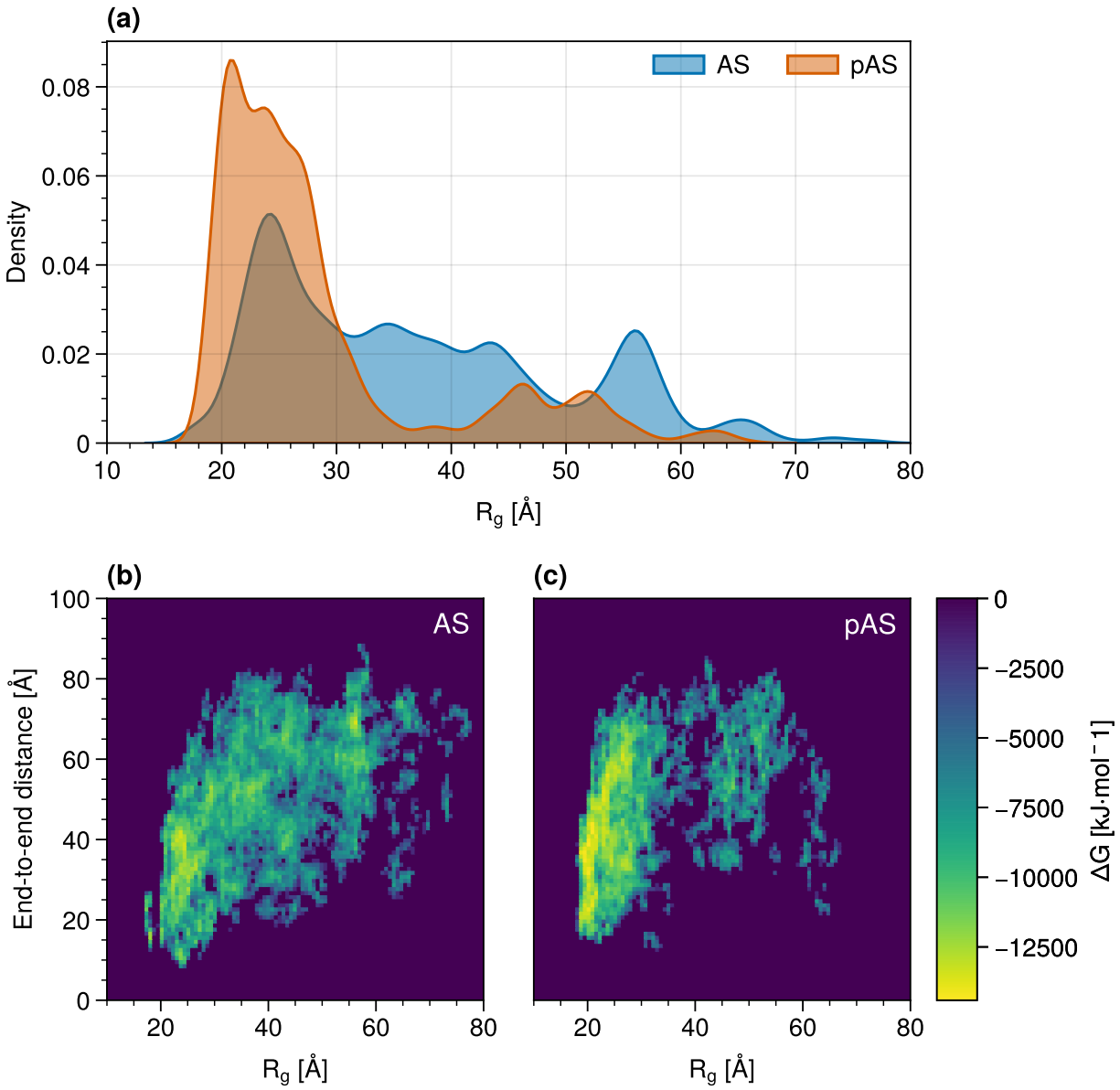

Figure 4: R_g distribution for AS (blue) and pAS (orange) (a) and the corresponding (highly approximate) free energy landscapes plotted as a function of the distance between the protein termini (b-c).

The solvent accessibility increases in the NAC region (Table 3). However, because of the large fluctuations of the C-terminus – N-terminus distances (Figure S8), this analysis is not conclusive.

The intramolecular interactions between the NAC region and the other regions slightly increase upon phosphorylation, as shown by the contact maps for each monomer and their

differences (Figure 5). Accordingly, the number of intramolecular hydrogen bonds increases (6(a-b)). However, one has to take these results with caution, as the number of such interactions shows a wide normal distribution with a large standard deviation (Table 2).

Table 3: Average Solvent Accessible Surface Area (SASA) in AS and pAS in the NAC region and at the N- and C-termini.

Protein	$SASA_N$ [Å^2]	$SASA_{NAC}$ [Å^2]	$SASA_C$ [Å^2]
AS	96 (± 41)	87 (± 31)	111 (± 32)
pAS	90 (± 42)	91 (± 32)	113 (± 39)

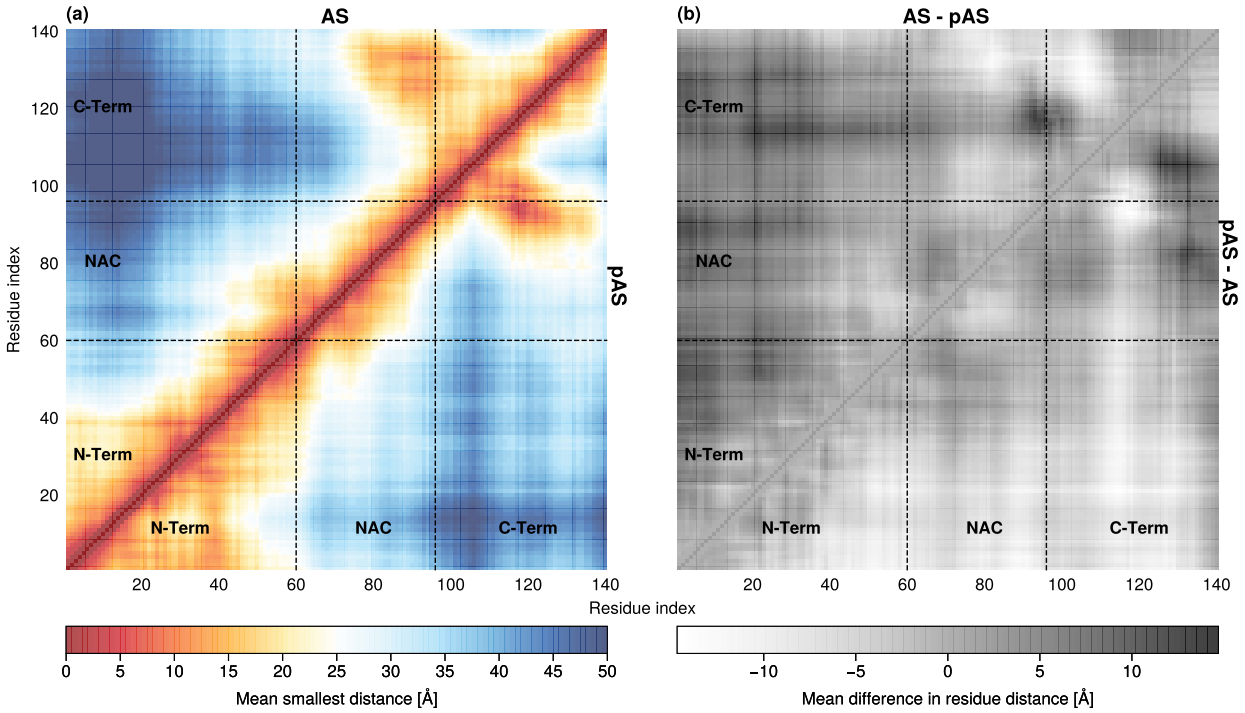

Figure 5: (a) Contact maps of AS (triangle above) and pAS (triangle below). (b) Mean residue distance differences between AS (triangle above) and pAS (triangle below).

These H-bonds are almost exclusively formed within every single domain (Figures 6(a-b)).

The number of salt bridges increases upon phosphorylation. The most persistent salt bridges common to both forms involve the N-term and NAC regions (K23–E20 and K58–E61, respectively, see Figures 6(a-b)). Few salt bridges are formed between the C-terminus and one of the two other domains. Of course, because the intramolecular contacts of IDPs are

labile, the scenario could be different over longer time scales or at different starting points.

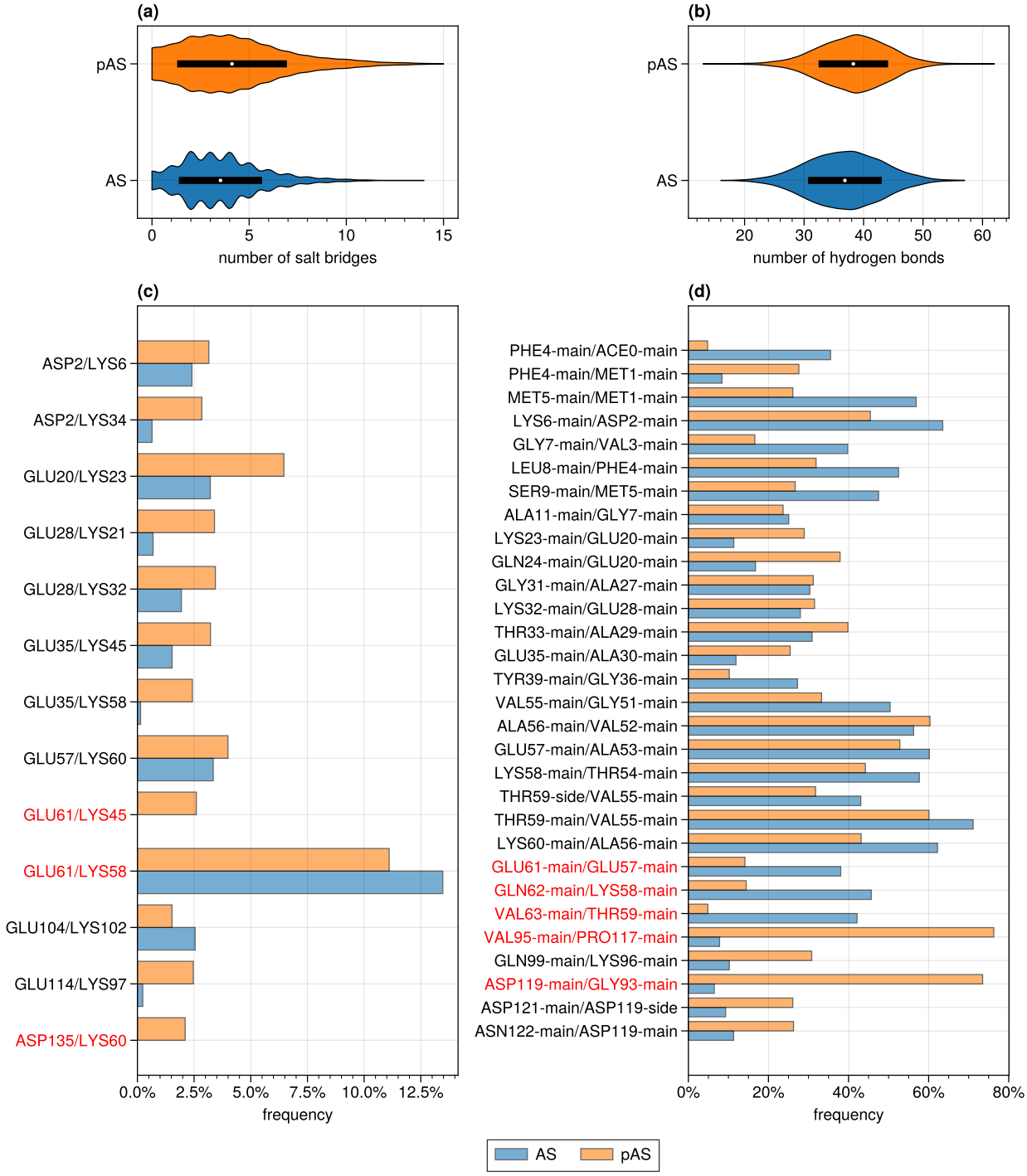

Figure 6: Distribution of the total number of salt bridges (a) and hydrogen bonds (b) in AS (blue) and pAS (orange). Frequency with which intradomain (black labels) and interdomain (red labels) salt bridges (a) and hydrogen bonds (b) are found in AS and pAS. Shown are salt bridges and hydrogen bonds that occur during at least 2 % and 25 % of the converged trajectory, respectively, in either the AS or pAS simulation.

We conclude that the protein's conformational ensemble becomes *slightly* more compact upon phosphorylation. This is associated with a small increase of intramolecular interactions. This is expected, as the increase of negative charge at the C-terminus can increase its interaction with the rest of the protein, and particularly with the positively charged N-terminus: the phosphate group interacts to a small extent with sodium ions (Figure S17) and, even less, with the protein residues (Figure S16). In fact, this group is fully solvent exposed, as shown by a plot of the phosphate oxygen-water oxygen radial distribution functions (RDFs) (Figure 7). This might be caused, at least in part, by the absence of surrounding basic residues. However, one has to take into account that the DES-Amber force field, and the a99SB-*disp* force field to an even greater extent, may overestimate the number of interacting water molecules (see Supplementary Information). Within these caveats, we suggest that the electrostatic field of the phosphate is strongly reduced by its solvation and does not impact the C-terminus-N-terminus interactions. This lack of interaction may also in part be explained by AS containing no arginine residues that are known to interact strongly with phosphate groups,[80] and indeed none of the lysine residues present in the N-terminal domain formed salt bridges with S129 during the simulation (Figure 6).

In AS, S129 interacts much less with the solvent than phosphate in pAS: The Oγ atom has only 2 water hydrogen (Figure 7) and no sodium ions in its surrounding. The serine oxydril group instead forms a variety of *intramolecular* H-bonds (with K80, K96, K97, K102, E126, E130 and E131 (Figure S16). S129 backbone units are observed to interact both with the solvent and nearby protein hydrogens in both AS and pAS.

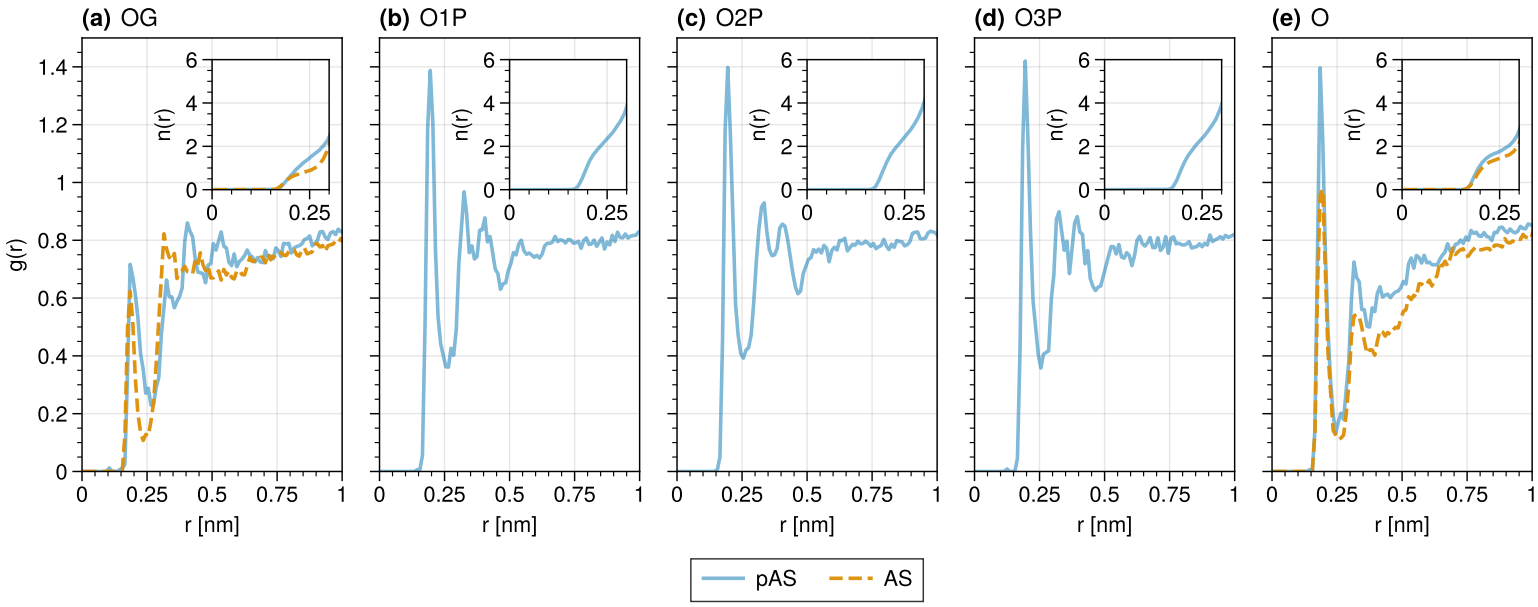

Figure 7: RDFs ($g(r)$) of the oxygen atoms of residue 129 and water hydrogens (a-e). Compare the RDF for pAS (blue) and AS (orange) for the oxygen atom in the side chain (a) and the carbonyl oxygen (e). (b-d) illustrate the RDF for the terminal phosphoryl oxygens. Insets show the integral of $g(r)$ up to 0.3 nm.

Thus, S129 forms many more intermolecular contacts than the phosphorylated residue in pAS.

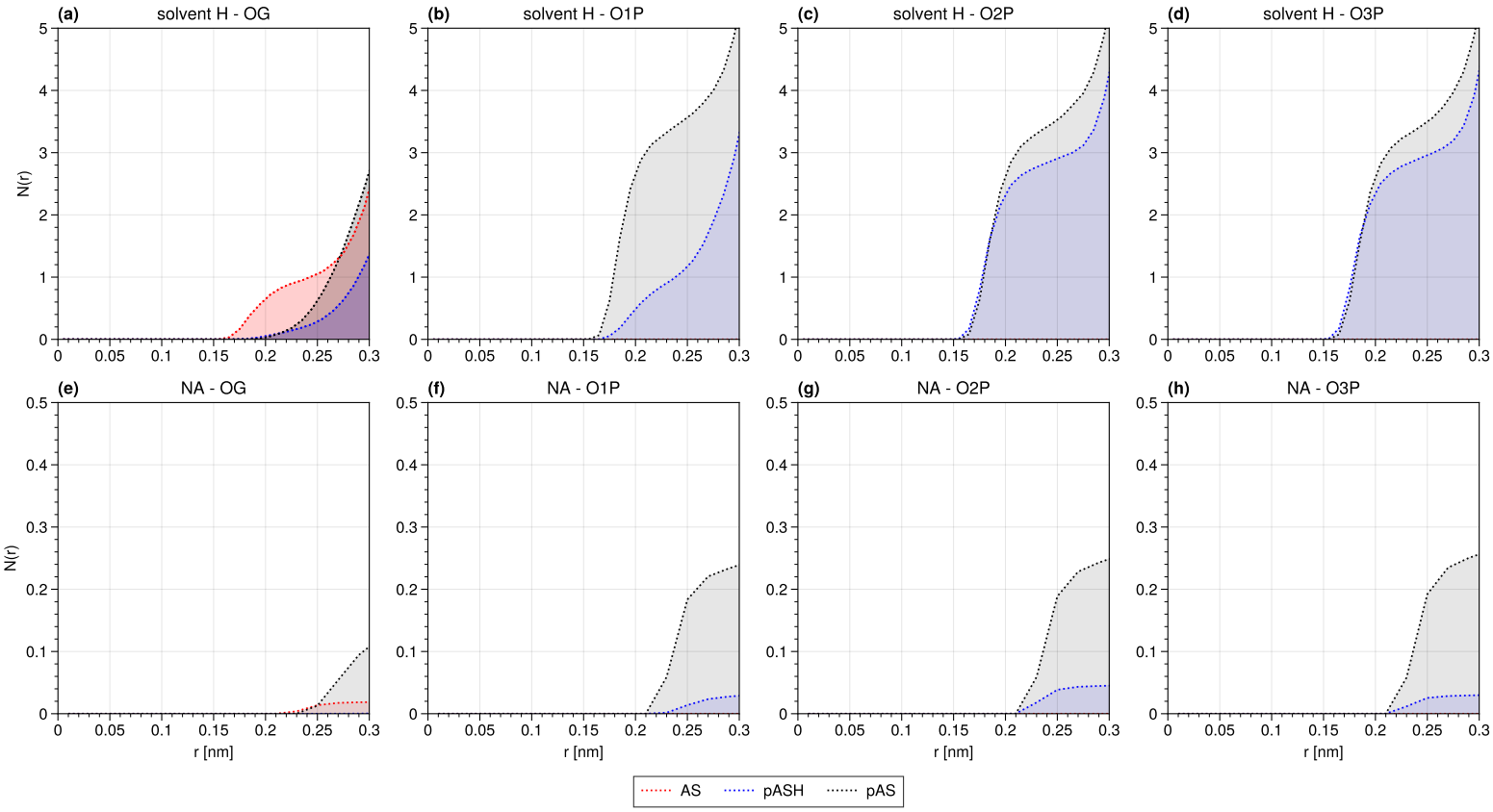

Figure 8: Coordination number ($n(r)$) of the oxygen atoms of residue 129 and both water hydrogens and sodium ions during the a99SB-*disp* simulations: calculated as integrals of the RDFs.

4 Conclusions

Because of the presence *in vivo* of phosphorylated AS, the detailed understanding of the impact of phosphorylation on this protein is important for informing therapeutic strategies aimed at targeting AS in synucleinopathies. Here, we investigated the effects of phosphorylation on the structural ensemble of AS in solution by REST2 simulations. pAS turns out not to undergo very large conformational changes relative to AS. It becomes slightly more compact than the unmodified protein.

Possibly, because the added phosphate moiety points towards the solvent (within the limitations of the force fields for the PTM), and interacts, to a lesser extent, with counte-

rions. However, our findings are consistent with the fact that CD spectra for AS do not change significantly upon S129 phosphorylation,[79] and with previous experimental data for AS showing that changes in the disordered C-terminal domain do not reflect any significant changes in the CD spectra.[78] As the overall helicity in AS is low, the sensitivity of the calculated CD spectra may not be sufficient to register any changes in pAS that are small in terms of overall secondary structure, yet large when compared to AS. Caution must therefore be exerted when comparing results from non-acetylated AS and physiological AS.[21]

Experimental data on pAS in solution is still lacking, hampering a direct comparison with our calculations.

Acknowledgement

TFO is supported by DFG (SFB1286-B8) and under Germany's Excellence Strategy - EXC 2067/1- 390729940.

This work was partially performed as part of the Helmholtz School for Data Science in Life, Earth and Energy (HDS-LEE) and received funding from the Helmholtz Association of German Research Centers.

Open Access publication funded by the Deutsche Forschungsgemeinschaft (DFG, German Research Foundation) – 491111487.

The authors gratefully acknowledge the Gauss Centre for Supercomputing e.V. (www.gauss-centre.eu) for funding this project by providing computing time through the John von Neumann Institute for Computing (NIC) on the GCS Supercomputer JUWELS at Jülich Supercomputing Centre (JSC).[81–84]

The authors gratefully acknowledge insightful discussions with Stefano Piana-Agostinetti regarding the choice of force field parameters, in particular with respect to the hydration of the phosphate group.

References

(1) Hou, Y.; Dan, X.; Babbar, M.; Wei, Y.; Hasselbalch, S. G.; Croteau, D. L.; Bohr, V. A. Ageing as a risk factor for neurodegenerative disease. *Nature Reviews Neurology* **2019**, *15*, 565–581.

(2) Rocca, W. A. The burden of Parkinson's disease: a worldwide perspective. *The Lancet* **2018**, *17*, 928–929.

(3) Lücking, C. B.; Brice, A. Alpha-synuclein and Parkinson's disease. *Cellular and Molecular Life Sciences CMLS* **2000**, *57*, 1894–1908.

(4) Baba, M.; Nakajo, S.; Tu, P.-H.; Tomita, T.; Nakaya, K.; Lee, V.; Trojanowski, J. Q.; Iwatsubo, T. Aggregation of alpha-synuclein in Lewy bodies of sporadic Parkinson's disease and dementia with Lewy bodies. *The American journal of pathology* **1998**, *152*, 879–884.

(5) Gibb, W.; Lees, A. The relevance of the Lewy body to the pathogenesis of idiopathic Parkinson's disease. *Journal of Neurology, Neurosurgery & Psychiatry* **1988**, *51*, 745–752.

(6) Nguyen, P. H.; Ramamoorthy, A.; Sahoo, B. R.; Zheng, J.; Faller, P.; Straub, J. E.; Dominguez, L.; Shea, J.-E.; Dokholyan, N. V.; De Simone, A., *et al.* Amyloid oligomers: A joint experimental/computational perspective on Alzheimer's disease, Parkinson's disease, type II diabetes, and amyotrophic lateral sclerosis. *Chemical reviews* **2021**, *121*, 2545–2647.

(7) Snead, D.; Eliezer, D. Alpha-synuclein function and dysfunction on cellular membranes. *Experimental neurobiology* **2014**, *23*, 292.

(8) Waudby, C. A.; Camilloni, C.; Fitzpatrick, A. W.; Cabrita, L. D.; Dobson, C. M.; Vendruscolo, M.; Christodoulou, J. In-cell NMR characterization of the secondary structure

populations of a disordered conformation of α-synuclein within E. coli cells. *PloS one* **2013**, *8*, e72286.

(9) Matsui, H.; Ito, S.; Matsui, H.; Ito, J.; Gabdulkhaev, R.; Hirose, M.; Yamanaka, T.; Koyama, A.; Kato, T.; Tanaka, M., *et al.* Phosphorylation of α-synuclein at T64 results in distinct oligomers and exerts toxicity in models of Parkinson's disease. *Proceedings of the National Academy of Sciences* **2023**, *120*, e2214652120.

(10) Ghanem, S. S.; Majbour, N. K.; Vaikath, N. N.; Ardah, M. T.; Erskine, D.; Jensen, N. M.; Fayyad, M.; Sudhakaran, I. P.; Vasili, E.; Melachroinou, K., *et al.* α-Synuclein phosphorylation at serine 129 occurs after initial protein deposition and inhibits seeded fibril formation and toxicity. *Proceedings of the National Academy of Sciences* **2022**, *119*, e2109617119.

(11) Wang, Y.; Shi, M.; Chung, K. A.; Zabetian, C. P.; Leverenz, J. B.; Berg, D.; Srulijes, K.; Trojanowski, J. Q.; Lee, V. M.-Y.; Siderowf, A. D., *et al.* Phosphorylated α-synuclein in Parkinson's disease. *Science translational medicine* **2012**, *4*, 121ra20–121ra20.

(12) Kawahata, I.; Finkelstein, D. I.; Fukunaga, K. Pathogenic Impact of α-Synuclein Phosphorylation and Its Kinases in α-Synucleinopathies. *International Journal of Molecular Sciences* **2022**, *23*, 6216.

(13) Oueslati, A.; Fournier, M.; Lashuel, H. A. Role of post-translational modifications in modulating the structure, function and toxicity of α-synuclein: implications for Parkinson's disease pathogenesis and therapies. *Progress in brain research* **2010**, *183*, 115–145.

(14) Ramalingam, N.; Jin, S.-X.; Moors, T. E.; Fonseca-Ornelas, L.; Shimanaka, K.; Lei, S.; Cam, H. P.; Watson, A. H.; Brontesi, L.; Ding, L., *et al.* Dynamic physiological α-synuclein S129 phosphorylation is driven by neuronal activity. *npj Parkinson's Disease* **2023**, *9*, 4.

(15) Xie, Y.; Jiang, Y.; Ben-Amotz, D. Detection of amino acid and peptide phosphate protonation using Raman spectroscopy. *Analytical biochemistry* **2005**, *343*, 223–230.

(16) Paleologou, K. E.; Schmid, A. W.; Rospigliosi, C. C.; Kim, H.-Y.; Lamberto, G. R.; Fredenburg, R. A.; Lansbury, P. T.; Fernandez, C. O.; Eliezer, D.; Zweckstetter, M., *et al.* Phosphorylation at Ser-129 but not the phosphomimics S129E/D inhibits the fibrillation of α-synuclein. *Journal of Biological Chemistry* **2008**, *283*, 16895–16905.

(17) Schreurs, S.; Gerard, M.; Derua, R.; Waelkens, E.; Taymans, J.-M.; Baekelandt, V.; Engelborghs, Y. In vitro phosphorylation does not influence the aggregation kinetics of WT α-synuclein in contrast to its phosphorylation mutants. *International journal of molecular sciences* **2014**, *15*, 1040–1067.

(18) Fauvet, B.; Fares, M.-B.; Samuel, F.; Dikiy, I.; Tandon, A.; Eliezer, D.; Lashuel, H. A. Characterization of Semisynthetic and Naturally Nα-Acetylated α-Synuclein in Vitro and in Intact Cells. *Journal of Biological Chemistry* **2012**, *287*, 28243–28262.

(19) Fujiwara, H.; Hasegawa, M.; Dohmae, N.; Kawashima, A.; Masliah, E.; Goldberg, M. S.; Shen, J.; Takio, K.; Iwatsubo, T. α-Synuclein Is Phosphorylated in Synucleinopathy Lesions. *Nature Cell Biology* **2002**, *4*, 160–164.

(20) Wang, L.; Friesner, R. A.; Berne, B. Replica exchange with solute scaling: a more efficient version of replica exchange with solute tempering (REST2). *The Journal of Physical Chemistry B* **2011**, *115*, 9431–9438.

(21) Rossetti, G.; Musiani, F.; Abad, E.; Dibenedetto, D.; Mouhib, H.; Fernandez, C. O.; Carloni, P. Conformational ensemble of human α-synuclein physiological form predicted by molecular simulations. *Physical Chemistry Chemical Physics* **2016**, *18*, 5702–5706.

(22) Palomino-Hernandez, O.; Buratti, F. A.; Sacco, P. S.; Rossetti, G.; Carloni, P.; Fernandez, C. O. Role of Tyr-39 for the Structural Features of α-Synuclein and for the

Interaction with a Strong Modulator of Its Amyloid Assembly. *International journal of molecular sciences* **2020**, *21*, 5061.

(23) Theillet, F.-X.; Binolfi, A.; Bekei, B.; Martorana, A.; Rose, H. M.; Stuiver, M.; Verzini, S.; Lorenz, D.; Van Rossum, M.; Goldfarb, D., *et al.* Structural disorder of monomeric α-synuclein persists in mammalian cells. *Nature* **2016**, *530*, 45–50.

(24) Robustelli, P.; Piana, S.; Shaw, D. E. Developing a molecular dynamics force field for both folded and disordered protein states. *Proceedings of the National Academy of Sciences* **2018**, *115*, E4758–E4766.

(25) Robustelli, P.; Ibanez-de Opakua, A.; Campbell-Bezat, C.; Giordanetto, F.; Becker, S.; Zweckstetter, M.; Pan, A. C.; Shaw, D. E. Molecular basis of small-molecule binding to α-synuclein. *bioRxiv* **2021**,

(26) Uluca, B.; Viennet, T.; Petrović, D.; Shaykhalishahi, H.; Weirich, F.; Gönülalan, A.; Strodel, B.; Etzkorn, M.; Hoyer, W.; Heise, H. DNP-enhanced MAS NMR: a tool to snapshot conformational ensembles of α-synuclein in different states. *Biophysical journal* **2018**, *114*, 1614–1623.

(27) Jain, K.; Ghribi, O.; Delhommelle, J. Folding free-energy landscape of α-synuclein (35–97) via replica exchange molecular dynamics. *Journal of Chemical Information and Modeling* **2020**, *61*, 432–443.

(28) Ilie, I. M.; Nayar, D.; Den Otter, W. K.; Van Der Vegt, N. F.; Briels, W. J. Intrinsic conformational preferences and interactions in α-synuclein fibrils: insights from molecular dynamics simulations. *Journal of chemical theory and computation* **2018**, *14*, 3298–3310.

(29) Chwastyk, M.; Cieplak, M. Conformational biases of α-synuclein and formation of transient knots. *The Journal of Physical Chemistry B* **2019**, *124*, 11–19.

(30) Perlmutter, J. D.; Braun, A. R.; Sachs, J. N. Curvature dynamics of α-synuclein familial parkinson disease mutants. *Journal of Biological Chemistry* **2009**, *284*, 7177–7189.

(31) Allison, J. R.; Varnai, P.; Dobson, C. M.; Vendruscolo, M. Determination of the free energy landscape of α-synuclein using spin label nuclear magnetic resonance measurements. *Journal of the American Chemical Society* **2009**, *131*, 18314–18326.

(32) Amos, S.-B. T.; Schwarz, T. C.; Shi, J.; Cossins, B. P.; Baker, T. S.; Taylor, R. J.; Konrat, R.; Sansom, M. S. Membrane Interactions of α-Synuclein Revealed by Multiscale Molecular Dynamics Simulations, Markov State Models, and NMR. *The Journal of Physical Chemistry B* **2021**, *125*, 2929–2941.

(33) Herrera, F. E.; Chesi, A.; Paleologou, K. E.; Schmid, A.; Munoz, A.; Vendruscolo, M.; Gustincich, S.; Lashuel, H. A.; Carloni, P. Inhibition of α-synuclein fibrillization by dopamine is mediated by interactions with five C-terminal residues and with E83 in the NAC region. *PloS one* **2008**, *3*, e3394.

(34) Robustelli, P.; Ibanez-de Opakua, A.; Campbell-Bezat, C.; Giordanetto, F.; Becker, S.; Zweckstetter, M.; Pan, A. C.; Shaw, D. E. Molecular basis of small-molecule binding to α-synuclein. *Journal of the American Chemical Society* **2022**, *144*, 2501–2510.

(35) Balesh, D.; Ramjan, Z., *et al.* Unfolded annealing molecular dynamics conformers for wild-type and disease-associated variants of alpha-synuclein show no propensity for beta-sheetformation. *Journal of Biophysical Chemistry* **2011**, *2011*.

(36) Allison, J. R.; Rivers, R. C.; Christodoulou, J. C.; Vendruscolo, M.; Dobson, C. M. A relationship between the transient structure in the monomeric state and the aggregation propensities of α-synuclein and β-synuclein. *Biochemistry* **2014**, *53*, 7170–7183.

(37) Dedmon, M. M.; Lindorff-Larsen, K.; Christodoulou, J.; Vendruscolo, M.; Dobson, C. M. Mapping long-range interactions in α-synuclein using spin-label NMR and

ensemble molecular dynamics simulations. *Journal of the American Chemical Society* **2005**, *127*, 476–477.

(38) Park, S.; Yoon, J.; Jang, S.; Lee, K.; Shin, S. The role of the acidic domain of α-synuclein in amyloid fibril formation: a molecular dynamics study. *Journal of Biomolecular Structure and Dynamics* **2016**, *34*, 376–383.

(39) Brodie, N. I.; Popov, K. I.; Petrotchenko, E. V.; Dokholyan, N. V.; Borchers, C. H. Conformational ensemble of native α-synuclein in solution as determined by short-distance crosslinking constraint-guided discrete molecular dynamics simulations. *PLoS computational biology* **2019**, *15*, e1006859.

(40) Tsigelny, I. F.; Bar-On, P.; Sharikov, Y.; Crews, L.; Hashimoto, M.; Miller, M. A.; Keller, S. H.; Platoshyn, O.; Yuan, J. X.-J.; Masliah, E. Dynamics of α-synuclein aggregation and inhibition of pore-like oligomer development by β-synuclein. *The FEBS journal* **2007**, *274*, 1862–1877.

(41) Ramis, R.; Ortega-Castro, J.; Casasnovas, R.; Mariño, L.; Vilanova, B.; Adrover, M.; Frau, J. A coarse-grained molecular dynamics approach to the study of the intrinsically disordered protein α-synuclein. *Journal of chemical information and modeling* **2019**, *59*, 1458–1471.

(42) Yu, H.; Han, W.; Ma, W.; Schulten, K. Transient β-hairpin formation in α-synuclein monomer revealed by coarse-grained molecular dynamics simulation. *The Journal of chemical physics* **2015**, *143*, 12B623_1.

(43) Narayanan, C.; Weinstock, D. S.; Wu, K.-P.; Baum, J.; Levy, R. M. Investigation of the polymeric properties of α-synuclein and comparison with NMR experiments: a replica exchange molecular dynamics study. *Journal of chemical theory and computation* **2012**, *8*, 3929–3942.

(44) Dibenedetto, D.; Rossetti, G.; Caliandro, R.; Carloni, P. A molecular dynamics simulation-based interpretation of nuclear magnetic resonance multidimensional heteronuclear spectra of α-synuclein· dopamine adducts. *Biochemistry* **2013**, *52*, 6672–6683.

(45) Tsigelny, I. F.; Sharikov, Y.; Miller, M. A.; Masliah, E. Mechanism of alpha-synuclein oligomerization and membrane interaction: theoretical approach to unstructured proteins studies. *Nanomedicine: Nanotechnology, Biology and Medicine* **2008**, *4*, 350–357.

(46) Zhang, T.; Tian, Y.; Li, Z.; Liu, S.; Hu, X.; Yang, Z.; Ling, X.; Liu, S.; Zhang, J. Molecular dynamics study to investigate the dimeric structure of the full-length α-synuclein in aqueous solution. *Journal of Chemical Information and Modeling* **2017**, *57*, 2281–2293.

(47) Savva, L.; Platts, J. A. How Cu (II) binding affects structure and dynamics of α-synuclein revealed by molecular dynamics simulations. *Journal of Inorganic Biochemistry* **2023**, *239*, 112068.

(48) Pedersen, K. B.; Flores-Canales, J. C.; Schiøtt, B. Predicting molecular properties of α-synuclein using force fields for intrinsically disordered proteins. *Proteins: Structure, Function, and Bioinformatics* **2023**, *91*, 47–61.

(49) Razzokov, J.; Fazliev, S.; Makhkamov, M.; Marimuthu, P.; Baev, A.; Kurganov, E. Effect of Electric Field on α-Synuclein Fibrils: Revealed by Molecular Dynamics Simulations. *International Journal of Molecular Sciences* **2023**, *24*, 6312.

(50) Piana, S.; Robustelli, P.; Tan, D.; Chen, S.; Shaw, D. E. Development of a force field for the simulation of single-chain proteins and protein–protein complexes. *Journal of chemical theory and computation* **2020**, *16*, 2494–2507.

(51) Khoury, G. A.; Thompson, J. P.; Smadbeck, J.; Kieslich, C. A.; Floudas, C. A. Forcefield_PTM: Ab initio charge and AMBER forcefield parameters for frequently occurring

post-translational modifications. *Journal of chemical theory and computation* **2013**, *9*, 5653–5674.

(52) Homeyer, N.; Horn, A. H.; Lanig, H.; Sticht, H. AMBER force-field parameters for phosphorylated amino acids in different protonation states: phosphoserine, phosphothreonine, phosphotyrosine, and phosphohistidine. *Journal of molecular modeling* **2006**, *12*, 281–289.

(53) Petrov, D.; Margreitter, C.; Grandits, M.; Oostenbrink, C.; Zagrovic, B. A systematic framework for molecular dynamics simulations of protein post-translational modifications. *PLoS computational biology* **2013**, *9*, e1003154.

(54) Zhong, B.; Song, G.; Chen, H.-F. Balanced Force Field ff03CMAP Improving the Dynamics Conformation Sampling of Phosphorylation Site. *International Journal of Molecular Sciences* **2022**, *23*, 11285.

(55) Margreitter, C.; Reif, M. M.; Oostenbrink, C. Update on phosphate and charged post-translationally modified amino acid parameters in the GROMOS force field. *Journal of computational chemistry* **2017**, *38*, 714–720.

(56) Vymětal, J.; Jurásková, V.; Vondrášek, J. AMBER and CHARMM force fields inconsistently portray the microscopic details of phosphorylation. *Journal of Chemical Theory and Computation* **2018**, *15*, 665–679.

(57) Rieloff, E.; Skepö, M. Phosphorylation of a disordered peptide—Structural effects and force field inconsistencies. *Journal of chemical theory and computation* **2020**, *16*, 1924–1935.

(58) Man, V. H.; He, X.; Gao, J.; Wang, J. Phosphorylation of Tau R2 Repeat Destabilizes Its Binding to Microtubules: A Molecular Dynamics Simulation Study. *ACS Chemical Neuroscience* **2023**,

(59) Tucker, M. R.; Piana, S.; Tan, D.; LeVine, M. V.; Shaw, D. E. Development of Force Field Parameters for the Simulation of Single- and Double-Stranded Dna Molecules and Dna-Protein Complexes. *The Journal of Physical Chemistry B* **2022**, *126*, 4442–4457.

(60) Steinbrecher, T.; Latzer, J.; Case, D. Revised AMBER parameters for bioorganic phosphates. *Journal of chemical theory and computation* **2012**, *8*, 4405–4412.

(61) Roche, J.; Ying, J.; Maltsev, A. S.; Bax, A. Impact of Hydrostatic Pressure on an Intrinsically Disordered Protein: A High-Pressure NMR Study of α-Synuclein. *ChemBioChem* **2013**, *14*, 1754–1761.

(62) DeLano, W. L., *et al.* Pymol: An open-source molecular graphics tool. *CCP4 Newsletter on protein crystallography* **2002**, *40*, 82–92.

(63) Piana, S.; Donchev, A. G.; Robustelli, P.; Shaw, D. E. Water Dispersion Interactions Strongly Influence Simulated Structural Properties of Disordered Protein States. *The Journal of Physical Chemistry B* **2015**, *119*, 5113–5123.

(64) Darden, T.; York, D.; Pedersen, L. Particle mesh Ewald: An N log (N) method for Ewald sums in large systems. *The Journal of chemical physics* **1993**, *98*, 10089–10092.

(65) Evans, D. J.; Holian, B. L. The nose–hoover thermostat. *The Journal of chemical physics* **1985**, *83*, 4069–4074.

(66) Andersen, H. C. Molecular dynamics simulations at constant pressure and/or temperature. *The Journal of chemical physics* **1980**, *72*, 2384–2393.

(67) Hess, B.; Bekker, H.; Berendsen, H. J.; Fraaije, J. G. LINCS: a linear constraint solver for molecular simulations. *Journal of computational chemistry* **1997**, *18*, 1463–1472.

(68) Appadurai, R.; Koneru, J. K.; Bonomi, M.; Robustelli, P.; Srivastava, A. Clustering Heterogeneous Conformational Ensembles of Intrinsically Disordered Proteins With

T-Distributed Stochastic Neighbor Embedding. *Journal of Chemical Theory and Computation* **2023**, *19*, 4711–4727.

(69) McGibbon, R. T.; Beauchamp, K. A.; Harrigan, M. P.; Klein, C.; Swails, J. M.; Hernández, C. X.; Schwantes, C. R.; Wang, L.-P.; Lane, T. J.; Pande, V. S. MDTraj: A Modern Open Library for the Analysis of Molecular Dynamics Trajectories. *Biophysical Journal* **2015**, *109*, 1528 – 1532.

(70) Han, B.; Liu, Y.; Ginzinger, S. W.; Wishart, D. S. SHIFTX2: significantly improved protein chemical shift prediction. *Journal of biomolecular NMR* **2011**, *50*, 43–57.

(71) Bulheller, B. M.; Hirst, J. D. DichroCalc—circular and linear dichroism online. *Bioinformatics* **2009**, *25*, 539–540.

(72) de Bruyn, E. SPEADI: Scalable Protein Environment Analysis for Dynamics and Ions (v1.0.0). 2022; `https://doi.org/10.5281/zenodo.7436713`.

(73) de Bruyn, E.; Dorn, A. E.; Zimmermann, O.; Rossetti, G. Speadi: Accelerated Analysis of Idp-Ion Interactions From MD-Trajectories. *Biology* **2023**, *12*, 581.

(74) Wernet, P.; Nordlund, D.; Bergmann, U.; Cavalleri, M.; Odelius, M.; Ogasawara, H.; Näslund, L. A.; Hirsch, T. K.; Ojamäe, L.; Glatzel, P.; Pettersson, L. G. M.; Nilsson, A. The Structure of the First Coordination Shell in Liquid Water. *Science* **2004**, *304*, 995–999.

(75) Donald, J. E.; Kulp, D. W.; DeGrado, W. F. Salt Bridges: Geometrically Specific, Designable Interactions. *Proteins: Structure, Function, and Bioinformatics* **2011**, *79*, 898–915.

(76) Kabsch, W.; Sander, C. Dictionary of protein secondary structure: pattern recognition of hydrogen-bonded and geometrical features. *Biopolymers: Original Research on Biomolecules* **1983**, *22*, 2577–2637.

(77) Lazar, T.; Guharoy, M.; Vranken, W.; Rauscher, S.; Wodak, S. J.; Tompa, P. Distance-Based metrics for comparing conformational ensembles of intrinsically disordered proteins. *Biophysical Journal* **2020**, *118*, 2952–2965.

(78) Maltsev, A. S.; Ying, J.; Bax, A. Impact of N-terminal acetylation of α-synuclein on its random coil and lipid binding properties. *Biochemistry* **2012**, *51*, 5004–5013.

(79) Samuel, F.; Flavin, W. P.; Iqbal, S.; Pacelli, C.; Renganathan, S. D. S.; Trudeau, L.-E.; Campbell, E. M.; Fraser, P. E.; Tandon, A. Effects of serine 129 phosphorylation on α-synuclein aggregation, membrane association, and internalization. *Journal of Biological Chemistry* **2016**, *291*, 4374–4385.

(80) Mandel-Gutfreund, Y.; Schueler, O.; Margalit, H. Comprehensive Analysis of Hydrogen Bonds in Regulatory Protein Dna-Complexes: in Search of Common Principles. *Journal of Molecular Biology* **1995**, *253*, 370–382.

(81) Krause, D. Juwels: Modular Tier-0/1 Supercomputer At Jülich Supercomputing Centre. *Journal of large-scale research facilities JLSRF* **2019**, *5*, A135.

(82) Alvarez, D. Juwels Cluster and Booster: Exascale Pathfinder With Modular Supercomputing Architecture At Juelich Supercomputing Centre. *Journal of large-scale research facilities JLSRF* **2021**, *7*, A183.

(83) Herten, A. JUWELS Booster - Early User Experiences. Proceedings of the 2021 on Performance EngineeRing, Modelling, Analysis, and VisualizatiOn STrategy. 2021; p nil.

(84) Kesselheim, S. *et al. Lecture Notes in Computer Science*; Lecture Notes in Computer Science; Springer International Publishing, 2021; pp 453–468.